



Vegetation of *Chamaecyparis montane* cloud forest in Lalashan Forest Dynamics Plot

Ting CHEN, Yi-Nuo LEE, Po-Yu LIN, Kun-Sung WU, David ZELENÝ*

*Institute of Ecology and Evolutionary Biology, National Taiwan University, Roosevelt Rd. 1, 106 17 Taipei, Taiwan. *Corresponding author's email: zeleny@ntu.edu.tw*

(Manuscript received 5 November 2023; Accepted 23 August 2024; Online published 3 September 2024)

ABSTRACT: To study how species composition and physiognomical structure of *Chamaecyparis montane* mixed cloud forest in Taiwan changes along main soil, topographical and microclimatic variables on a small scale, we established a 1-ha Lalashan Forest Dynamics Plot in northern Taiwan (24°43' N, 121°26' E, elevation 1758–1782 m a.s.l.). Plot is affected by prevailing NE wind direction related to winter monsoon, and by seasonal fog frequency with highest fog density in autumn and winter. We finished the first census of all woody species in August 2020, and collected environmental factors related to soil and topographical properties, measured microclimate and soil moisture within the plot. In total, we recorded 5220 individuals with diameter at breast height ≥ 1 cm. These belong to 65 species, 42 genera and 29 families, with a basal area of 69.1 m² ha⁻¹, and are dominated by *Chamaecyparis obtusa* var. *formosana*, *Rhododendron formosanum* and *Quercus sessilifolia*. Modified TWINSpan classified vegetation into three types (ridge, east-facing slope and valley). Unconstrained ordination showed that the main gradients behind species composition changes are related to windwardness and convexity. Both east-facing slope type and valley type have relatively lower temperatures than ridge type, especially during summer. Convexity is related to soil moisture gradient (from dryer convex to wet concave sites). From soil properties, pH is negatively and phosphorus is positively related to topographical convexity. Collected data will serve as a baseline for future resurveys and monitoring changes within this montane cloud forest.

KEY WORDS: DCA, microclimatic measurements, modified two-way indicator species analysis, northeast winter monsoon.

INTRODUCTION

Montane cloud forests (MCFs) are characterised by the presence of persistent and frequent wind-driven cloud and foggy conditions at the ground (tree) level (Hamilton 1995). The distribution of montane cloud forests is highly fragmented according to the distribution of persistently foggy zones, making these fragments act like isolated islands which are assumed to promote speciation and endemism (Bruijnzeel *et al.*, 2011; Li *et al.*, 2015). MCFs are one of the world's most endangered ecosystems because of their sensitivity to changes in unique ecological conditions (Bruijnzeel *et al.*, 2011). In addition, climate observations show that MCFs are suffering from a decreasing trend in ground fog occurrence which is likely related to climate change (Still *et al.*, 1999; Foster, 2001; Ponco-Reyes *et al.*, 2012; Hu and Riveros-Iregui, 2016).

High fog frequency in montane cloud forests is responsible for the occurrence of special environmental conditions that are different from other forest types. These include horizontal precipitation, high air humidity, lower light availability, lower air temperature, and chronic nutrient limitation in soil (Stadtmüller, 1987). Horizontal precipitation represents an extra water input, in addition to rainfall (vertical precipitation), and is formed when fog condensates on leaf surfaces, a process also known as "fog stripping" (Stadtmüller, 1987). High air humidity mitigates the temperature differences, however, it hinders the leaf transpiration process and makes epiphylls (including lichens, mosses, algae, and fungi) grow on and cover the

leaves more easily, which may result in reduced photosynthesis (Lai *et al.*, 2006). The presence of fog can reduce 10–15% of light compared to no-fog conditions, causing lower light availability for plants, and hence, lower photosynthetic rate, but may lower the effect of photoinhibition and increase photosynthesis efficiency under diffuse light at the same time (Urban *et al.*, 2007; Reinhardt and Smith, 2008). When fog occurs, the air temperature is 3–6°C lower than analogous site without fog, alleviating possible heat stress for plants; however, plants may occasionally encounter frost events. Lower air temperature may also lead to a relatively low overall amount of heat received by plants, thus decreasing photosynthesis efficiency (Lai *et al.*, 2006). Due to frequent high air/soil humidity and lower air temperature, the decomposition rates in montane cloud forests are slower, possibly causing chronic nutrient limitation in soil (Tanner *et al.*, 1990).

Past studies about montane cloud forests were mostly focusing on tropical regions (Stadtmüller, 1987), and only a few were done in subtropical montane cloud forests (SMCF), although their biological and conservation value is not less significant (Li *et al.*, 2015). In subtropical eastern Asia, a large proportion of montane cloud forests are evergreen broadleaved forests mixed with coniferous and deciduous broadleaved trees (Su, 1984; Li *et al.*, 2015), while tropical montane cloud forests are dominated only by evergreen broad-leaved trees (Bruijnzeel *et al.*, 2011).

Zonal forests in Taiwan can be classified into five vegetative zones based on local climate, primarily driven



by elevation (Li *et al.* 2013). At elevations around 1500 to 2500 m a.s.l., the montane zone is characterised by frequent ground fog occurrence (Li *et al.*, 2015; Schulz *et al.*, 2017). In some areas, montane cloud forests are distributed in lower elevations than 1500 m a.s.l., partly due to the influence of the northeastern monsoon, which locally decreases the temperature, especially in the northeast part of Taiwan (Lai *et al.*, 2006; Li *et al.*, 2013, 2015; Schulz *et al.*, 2017), and also as the result of the mass elevation heating effect (Massenerhebung effect, Quervain *et al.*, 1904), which decreases the elevation of vegetation zones on smaller and isolated mountains as a result of lower heating effect (Su, 1984). Montane cloud forests in Taiwan include three main subtropical vegetation types, namely *Chamaecyparis* montane mixed cloud forest, *Fagus* montane deciduous broad-leaved cloud forest, and *Quercus* montane evergreen broad-leaved cloud forest, and one tropical vegetation type, *Pasania-Elaeocarpus* montane evergreen broad-leaved cloud forest (Li *et al.*, 2013).

Detailed forest dynamics plot (FDP) studies allow us to better understand the forest ecosystems, and with long-term plot resurveys, we can also monitor vegetation dynamics in the sense of species composition change in time. This is essential for improving theoretical knowledge about the dynamics of the montane cloud forest vegetation and describing their response to ongoing climate change. In Taiwan, there are three previous FDP studies focusing on the SMCF: one in Yuanyang Lake Long-Term Ecological Research Site (Chou *et al.*, 2000), and two in Mt. Peitungyen in central Taiwan (Song, 1996; Song *et al.*, 2010; Hu and Tzeng, 2019). However, although northeastern monsoon has been considered in lowering the elevation of montane cloud forest in certain parts of Taiwan, none of these studies studied the effect of monsoon. On the contrary, the monsoon's effect on forest has been found in other Taiwanese FDP studies below the cloud zone, including the FDPs in lowland subtropical rainforest in Nanjenshan and Lanjenchi (Chao *et al.*, 2007, 2010). The forests under different wind exposure showed different species composition, and windward forests have denser, shorter, and smaller trees than leeward forests (Ku *et al.*, 2021). Thus, we thought it may be interesting to establish an FDP in the monsoon-exposed SMCF for better ecological understanding of fog and wind effect on vegetation, and for long-term monitoring.

We focus on *Chamaecyparis* montane mixed cloud forest, where coniferous and broad-leaved woody species co-occur, with an admixture of deciduous species (Li *et al.*, 2015). In 2019, we established the Lalashan Forest Dynamics Plot (LFDP) on a flat ridge with an east-facing slope influenced by the northeastern monsoon in northern Taiwan. This study reports the results of our first vegetation survey of woody species composition and its relationship to measured environmental variables. The

aims of our study were: 1) to distinguish the main vegetation types within the dynamics plot and describe their compositional and environmental differences; 2) to describe the main gradients of changes in woody species composition within the forest dynamics plot and underlying environmental variables; and 3) to explore environmental conditions of the plot, including soil chemical properties, topography and microclimatic conditions. These results will serve as baseline data for future resurveys.

MATERIAL AND METHODS

Study site description

Lalashan Forest Dynamics Plot (LFDP; 24°43' N, 121°26' E; elevation 1758–1782 m a.s.l.) is located on a wide part of the mountain ridge near the saddle between Lalashan and Tamanshan, inside the Chatianshan Nature Reserve, in northern Taiwan (Fig. 1A&B). The mountain ridge is in the northern branch of Xueshan Range, with orientation of northwest-southeast direction. There are two west-east direction ephemeral streams in the western part of LFDP and an east-facing slope exposed to the northeastern monsoon in the eastern part of LFDP (Fig. 1C). The forest appears to be intact, not influenced by any type of silvicultural management, and except for a small treeless opening in the saddle (with our weather station), it is part of a continuous forest stand. The vegetation in LFDP is *Chamaecyparis* montane mixed cloud forest (Li *et al.*, 2013), which is dominated by *Chamaecyparis obtusa* var. *formosana* (coniferous species) and *Rhododendron formosanum* (evergreen broadleaf species). Microclimatic conditions, measured by Lalashan Saddle weather station between January 1 and December 31, 2021, are the following. Mean annual precipitation was 4024 mm/yr⁻¹. The mean annual temperature was 13.7 °C, the mean monthly temperature of the warmest month (July) was 18.9 °C, and the mean monthly temperature of the coldest month (January) was 4.8 °C (Fig. 1D). Frost events occurred in January, February, and December. The prevailing wind direction was mainly from the northeast (around 60°) and occasionally also from the southwest (around 240°; Fig. 1E). The number of foggy days (i.e. days with at least one measurement of visibility below 1000 m) was 335 days in average per year, and the total duration time of fog was 35.0% of the time of year. The month with the highest fog frequency was November 2021, and the lowest was March 2021 (Fig. 1F). Details about the weather station measurements are in the Supplement.

Sampling design

We established the boundaries of the plot and all subplots in July 2019 and finished the first census of woody species in August 2020. The establishment and survey of woody species followed the Forest Global Earth

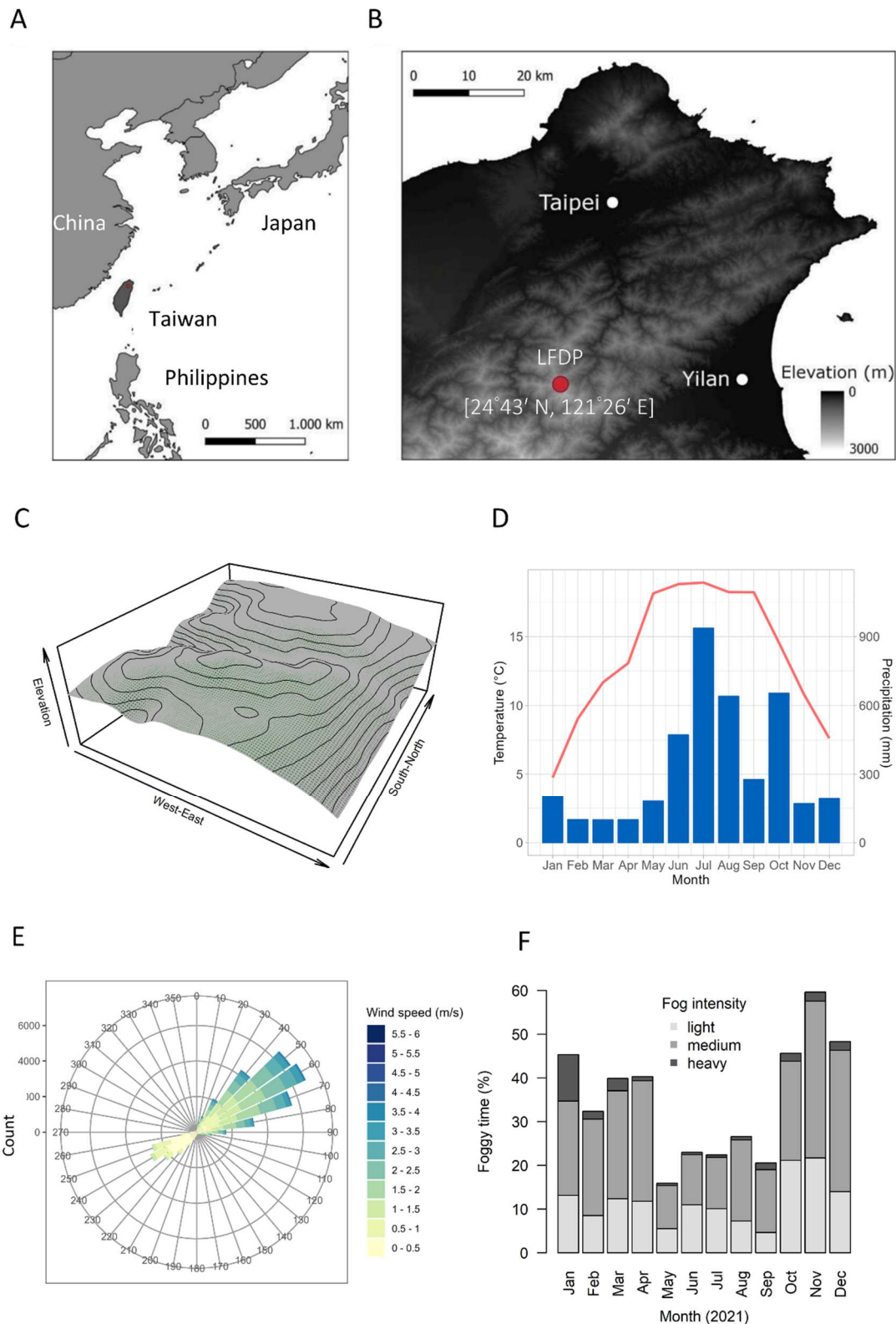


Fig. 1. Location of LFDP (red point) in **A.** East Asia and in **B.** northern Taiwan. **C.** Three-dimensional map of the LFDP. **D.** Monthly temperatures (red curve, scale on the left) and precipitations (blue bars, scale on the right), measured by Lalashan Saddle weather station. **E.** Wind rose charts from Lalashan Saddle weather station. **F.** Percentages of different fogginess intensity, as measured by visibility logger (light fogginess represents visibility from 500 to 1000 m, medium fogginess from 100 to 500 m, and heavy fogginess from 0 to 100 m). All microclimatic measurements in (C-E) were recorded between January 1, 2021, and December 31, 2021.

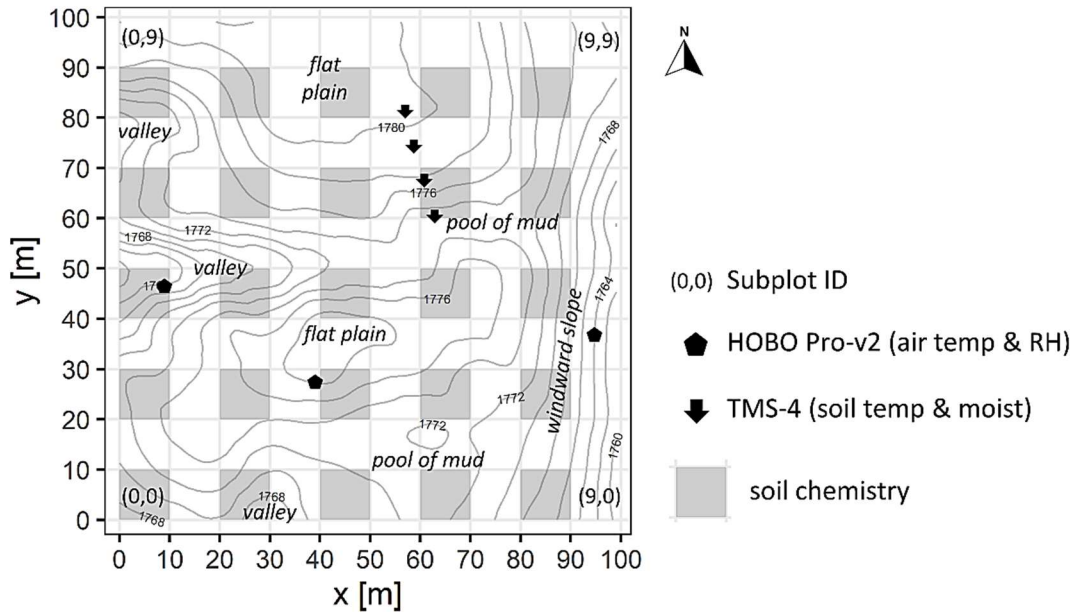


Fig. 2. Map of the Lalashan Forest Dynamics Plot with the positions of HOBO Pro-v2 loggers (air temperature and relative humidity, RH), TMS-4 loggers (soil temperature and moisture), and highlighted subplots where soil chemistry was measured. Text labels highlight typical topographical features of the plot.

Observatory Network (ForestGEO) Tree Census Protocol (Condit, 1998). We used the compass with transiting telescope (Ushikata LS-25, Kantum Ushikata Co. Ltd., Yokohama, Japan) to delineate a projected area of one hectare ($100\text{ m} \times 100\text{ m}$), which was then subdivided into $100\text{ m} \times 10\text{ m}$ subplots (Fig. 2). The aspect of the main LFDP axis is pointing to the north. The corners of the subplots were coded with the coordinates, with (0,0) starting from the southwest corner and ending with (10,10) in the northeast corner. The corners of the subplots were marked with PVC poles painted red at the top, and the centres of the subplots were marked with plastic poles painted yellow at the top. The subplot IDs were coded according to the coordinates of their southwest corners.

Species composition

When surveying, we first delineated the boundaries of each subplot with a tape, and only the trees rooted inside the surveyed subplot were recorded for the subplot. In each subplot, all individuals of woody species (excluding lianas) with a diameter at breast height (DBH) $\geq 1\text{ cm}$ were identified, tagged with an iron tag with a stamped number, mapped, and their DBH measured. If the individual tree had any branches with DBH $\geq 1\text{ cm}$, we also measured them and tagged them with a white plastic tag with a number written by a pencil.

For each species in each subplot, we calculated the importance value index (IVI; Curtis, 1959) using relative basal area (BA) and relative individual density. The BA (m^2ha^{-1}) of an individual was calculated from DBH of its main stem as $BA = 2 * (DBH/2)^2$; if the individual had any branches, BA was calculated separately for each of

them and summed together with the main stem. The relative basal area (%) of species i was calculated as the sum BA of all individuals of species i in the subplot divided by the sum of BA of all species in the subplot and multiplied by 100. The relative individual density (%) of species i was calculated as the count of individuals of species i (only the main stem was considered an individual) divided by the count of all species individuals and multiplied by 100. IVI of species i was then calculated as the sum of the relative basal area and relative individual density of species i , divided by two.

For each subplot, we calculated the density of individuals (as the number of all main stems in the subplot; individuals/ 100 m^2), total BA (as the sum of BA of all species in the subplot; m^2ha^{-1}), maximal BA (the BA of the tree with highest DBH; m^2ha^{-1}), mean DBH (for each individual we summed BA of main stem and all branches, if any, and recalculated it back to individual DBH, and then calculated mean of individual DBH in the subplot; cm) and the mean number of branches per individual (branch.ind $^{-1}$). The species in LFDP were categorised into three leaf types, including conifer, deciduous broadleaf and evergreen broadleaf species, using information from Flora of Taiwan, 2nd edition (Huang and Hsieh 1994–2003) and our field observations. Using leaf type category, for each subplot, we calculated BA of all conifer species, all deciduous species and all evergreen broadleaf species.

Topographical variables

The environmental factors related to topography, including elevation, convexity, slope, aspect and variables calculated from them (such as northeasterliness and



windwardness), were all derived from the elevation of the poles in corners of subplots. We first measured the absolute elevation of the pole (5,0) using GPS (GARMIN GPSMAP 64st, USA). Elevations of all other poles were calculated using this absolute elevation and slope angles between poles, which were recorded while delineating the plot. Then, for each subplot, the elevation was calculated as the mean elevation of its four corner poles. The convexity (Valencia *et al.*, 2004) was calculated as the elevation of the given subplot minus the mean elevation of its eight surrounding subplots; for marginal subplots, it was calculated as the elevation of the subplot's centre pole (additionally measured in the field using the compass with transiting telescope) minus the elevation of the subplot (calculated as the mean elevation of the four corner poles). The slope was calculated as the mean angular deviation from the horizon of each of the four triangular planes formed by connecting three of the target subplot's corner poles. The aspect was calculated as the elevation of the midpoints of each subplot's four sides by averaging the elevation of the two corner poles on each side, using the formula $180 - \arctan(fy / fx) (180 / \pi) + 90 (fx / |fx|)$, where fx is the midpoint elevation change from the east side to west side, and fy is the midpoint elevation change from the north side to south side (Valencia *et al.*, 2004, De Cáceres *et al.*, 2012). For analysis, we converted aspect into northeasterliness by folding it along the SW-NE direction (with 0° for SW and 180° for NE). The windwardness was calculated by multiplying the aspect, folded along the E-W axis (of prevailing wind) and centred around zero (by setting $+90^\circ$ in the east and -90° in the west), by slope; the highest values are in steeper, east facing slopes that are the most wind-affected, while the lowest values are in steeper west facing slopes, which are sheltered from the wind.

Soil properties

Selected physical and chemical soil properties were measured in each of the 100 subplots within the plot, with some more comprehensive measurements restricted only to the subset of 25 subplots. Each $10\text{ m} \times 10\text{ m}$ subplot was divided into four $5\text{ m} \times 5\text{ m}$ quadrats, and soil was treated in the centers of these quadrats. The soil properties measured in all 100 subplots include soil depth and rockiness. Soil depth was measured with a 30 cm long iron rod, 0.6 cm in diameter, with values ranging from 0–30 cm (values higher than 30 cm were recorded as 30+ cm). The measured values were converted into an ordinal scale (0 = 0 cm; 1 = 1–5 cm; 2 = 6–10 cm; 3 = 11–20 cm; 4 = 21–30 cm; 5 = 30+ cm), and median of the four values within each subplot was calculated to represent subplot-level soil depth. Soil rockiness was estimated as the relative proportion of stones in the soil when taking the soil samples, with values from four estimates per subplot averaged into one value. To measure the chemical properties of the soil, we collected four soil samples

within each subplot with an iron shovel from a depth of 0–10 cm after removing the surface litter and mixed into one mixed soil sample. The collected soil samples were air-dried in the lab for several weeks and sieved through a 2.0 mm sieve (2.0 mm laboratory test sieve, Endecotts Ltd, England). From all 100 samples, we measured soil pH, using a glass electrode pH meter (LAQUA F-71, Horiba Ltd., Kyoto, Japan) in the solution of soil sample and deionised water in 1:2 ratio (10 g of soil and 20 ml of deionised water). All other soil properties listed below were measured in the soil from a subset of 25 subplots. Soil texture (sand, silt and clay) was measured by hygrometer method (Gee and Bauder, 1986); organic C content was acquired by Walkley and Black dichromate method (Nelson and Sommers, 1996); total N was determined by Kjeldahl method (Nelson and Sommers, 1972); C/N ratio was calculated as organic C divided by total N; exchangeable N, which contained the ammonium-N and nitrate-N, was determined by KCl extraction and steam distillation (Mulvaney, 1996); available P was determined by Bray No. 1 method (modified from Burt, 2004) with a spectrometer (UV-1900PC, Macylab Instruments Inc., Shanghai, China); exchangeable cations of K, Ca and Mg were extracted by 1 M ammonium acetate (pH 7) and determined by a flame atomic absorbance spectrophotometer (AAnalyst 200, PerkinElmer, Inc., Waltham, MA, USA; Burt, 2004); and available cations of Fe, Mn, Cu, Zn were extracted by 0.1 N HCl and determined by AAnalyst 200 (Baker and Amacher, 1982). Note that we are aware that since the analysis was done on air-dried soil samples several months after these were collected in the field, for some of the chemical variables (namely those related to inorganic N), the measurements are less reliable and we do not consider them for interpretation (Turner and Romero, 2009).

Microclimatic measurements within the plot

To quantify air and soil microclimatic parameters of the studied forest, we 1) installed air temperature and relative humidity loggers within the dynamics plot to describe differences between the vegetation types, and 2) installed soil moisture loggers within the dynamics plot along the convex-concave topographical gradient.

Within the dynamics plot, we installed three HOBO Pro-v2 loggers housed in the sunshield RS1 (Onset Computer Corp. USA) by attaching them by zip ties on the northern side of a selected tree at the height of 1.4 m. The location was chosen to measure microclimate in the three alternative topographical positions (Fig. 2): valley in subplot (0,4), flat ridge in subplot (3,2), and east-facing wind-affected slope in subplot (9,3). Recording was conducted continuously from April 2020, with temperature and relative humidity recorded every 30 minutes. However, the logger sensor in the flat ridge was broken from October 2020 to June 2021.

Soil moisture and temperature were monitored by



installing four TMS-4 loggers (TOMST, Czech Republic) along the topographical gradient from the convex ridge to concave valley close to the centre of the dynamics plot (Fig. 2). The measurement was done from April 17 till May 28, 2022, every 15 minutes, and included soil moisture and three values of temperature: 15 cm above soil surface, 2 cm above soil surface and 6 cm below the surface.

Statistical analyses

Since some of the soil variables used for the analysis had skewed distribution, we transformed them by \log_{10} transformation to improve their distribution (organic C, total N, C/N ratio, exchangeable N, available P, K, Ca, Mg, Cu and Zn). Pairwise correlations among pairs of soil variables were calculated using Spearman's rank correlation coefficient.

With subplot-based IVI data, we classified the forest vegetation at LFDP into three vegetation types by modified two-way indicator species analysis (modified TWINSpan; Hill, 1979; Roleček *et al.*, 2009), using R package "twinspanR" (Zelený, 2021). Since the TWINSpan algorithm is restricted to presence-absence species composition data only, abundance data were transformed into a set of "pseudospecies" first, i.e. artificial species that aims to increase the importance of the species in analysis by multiplying its presence (according to cut levels of IVI set to 0, 2, 5, 10, and 20%). To quantify the compositional heterogeneity of individual clusters before their further division, we used the mean Bray-Curtis distance among plots within the same cluster. For species composition differences between the three vegetation types, we determined diagnostic, dominant and constant species for each vegetation type using JUICE software (Tichý, 2002). In the subplots of given vegetation type, diagnostic species were determined as species with fidelity coefficient $\Phi \geq 35$ (Chytrý *et al.*, 2002) significant at $P < 0.05$ when tested by Fisher's exact test. Dominant species were determined as species with $IVI \geq 20\%$, and constant species were determined as species with frequency $\geq 80\%$. Each vegetation type was named by a combination of the diagnostic species with the highest fidelity and the most dominant species for this vegetation type. Physiognomic and environmental differences between the three vegetation types were tested by analysis of variance (ANOVA) and Tukey's honestly significant difference test (Tukey's HSD). The F-test in ANOVA was adjusted for spatial autocorrelation by toroidal shift permutation test (399 permutations).

To explore the main compositional gradients in the species composition of the plot, we calculated detrended correspondence analysis (DCA; Hill and Gauch, 1980) on IVI data transformed as $\log_{10}(x + 1)$. We calculated multiple regression of each environmental variable on the first two DCA axes, including variables measured in all 100 subplots and those measured in the subset of 25 subplots, and projected them onto the ordination diagram

if they were significant (at $P < 0.05$ for variables measured in all 100 subplots, and at $P < 0.1$ for those measured in 25 subplots). We also visually verified the relationships between the three vegetation types and environmental factors by projecting them onto the DCA ordination diagram. The relationship of environmental variables to DCA axes was calculated as multiple regression by *envfit* function in "vegan" package (version 2.6-2, Oksanen *et al.*, 2022). To account for spatial autocorrelation, P-values were calculated by Monte Carlo permutation test with toroidal shift restricted permutation (Legendre and Legendre 2012), implemented within the "permut" package (version 0.9-7, Simpson, 2022).

The air temperatures and relative humidity (RH) measured by HOBO Pro-v2 loggers within the LFDP from August 1, 2021 to July 31, 2023 were aggregated into mean monthly temperature, mean monthly daily temperature deviation from ridge logger (which is comparatively the warmest from all three), and the proportion of wet days (i.e. days with $RH > 99\%$) and dry days ($RH < 75\%$). The soil moisture measured from April 20 to May 20, 2022, was recalculated into mean daily soil moisture and volumetric water content.

All analyses in this study were done in R program version 4.3.0 (R Core Team, 2023), with R code, vegetation data and environmental variables stored in the GitHub repository (<https://github.com/zdealveindy/LFDP-vegetation>).

RESULTS

A total of 5220 individuals belonging to 65 species, 42 genera and 29 families were recorded in LFDP, with a total BA of $69.1 \text{ m}^2 \text{ ha}^{-1}$. The surveyed forest is dominated by *Chamaecyparis obtusa* var. *formosana* (14% of the whole-plot-based IVI), *Rhododendron formosanum* (14%), *Quercus sessilifolia* (9%), *Trochodendron aralioides* (7%) and *Eurya crenatifolia* (5%), with the cumulative IVI of these five most dominant species reaching 49%. Distribution maps drawn separately for coniferous, deciduous and evergreen broadleaf species (Fig. 3) show proportional differences between each leaf-habit type (with 4499 evergreen broadleaf, 447 deciduous, and 270 coniferous individuals), and also different patterns of their distribution. Conifers are distributed mainly on the flat plateaus while avoiding the valleys and steep east-facing slopes, deciduous species frequently occur on steep east-facing slopes and also extend to ridges, and evergreen broadleaf species are scattered across the whole plot, with visibly higher individual density in the eastern part. When considering individual $10 \text{ m} \times 10 \text{ m}$ subplots (Fig. S3), species richness varied between 7 and 31 species, with median of 15; numbers of individuals varied between 11 and 184, with median of 41; sum of BA per subplot (recalculated per hectare) varied between $5.5 \text{ m}^2 \text{ ha}^{-1}$ and $191.6 \text{ m}^2 \text{ ha}^{-1}$, with average $69.1 \text{ m}^2 \text{ ha}^{-1}$; maximal BA of the largest tree within the subplot varied

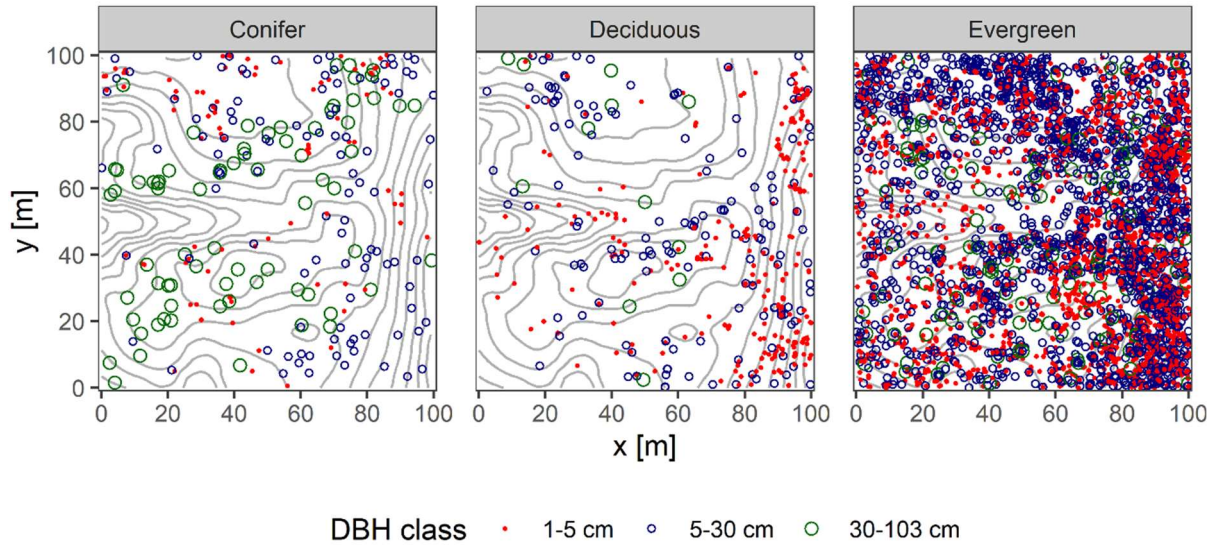


Fig. 3. Distribution map of conifer, deciduous and evergreen tree individuals stratified into three DBH classes (1-5 cm, 5-30 cm, and 30-103 cm).

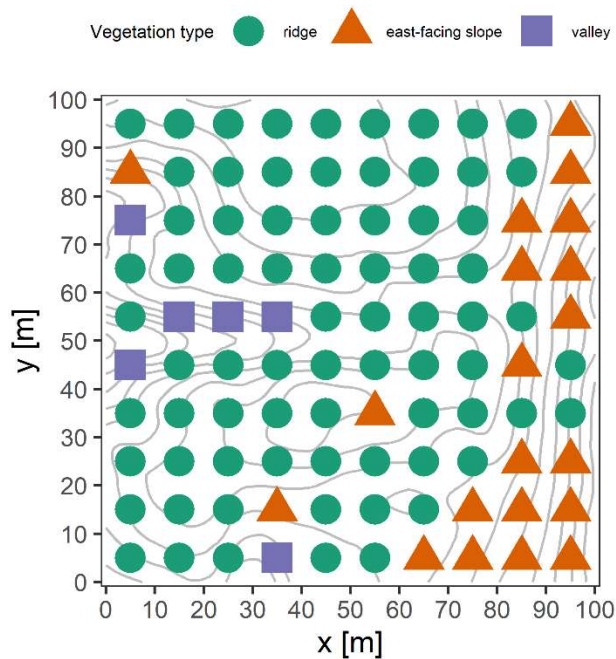


Fig. 4. Distribution of the three vegetation types at the subplot level in LFDP.

between 138.9 cm² and 8300.0 cm², with average 2170.3 cm²; the mean number of branches per individual varied between 0.1 and 2.1, with average of 0.6.

The three vegetation types, distinguished by modified TWINSPLAN, were named according to their typical topographical features and by the combination of the most diagnostic and the most dominant species as follows: (1) ridge type (*Daphniphyllum himalayense* subsp. *macropodum*-*Chamaecyparis obtusa* var. *formosana*), (2) east-facing slope type (*Pourthiaea villosa* var. *parvifolia*-*Rhododendron formosanum*) and (3) valley type

(*Hydrangea angustipetala*-*Eurya crenatifolia*) (Fig. 4).

Ridge type (74 subplots) is mostly distributed in the subplots on the broad ridge in the west and middle part of LFDP. Diagnostic species include *Daphniphyllum himalayense* subsp. *macropodum* and *Rhododendron formosanum* (listed by decreasing fidelity; Supplement: Table S1); dominant species include *Rhododendron formosanum*, *Chamaecyparis obtusa* var. *formosana*, *Quercus sessilifolia*, *Trochodendron aralioides*, *Prunus transarisanensis*, *Quercus longinix*, *Ilex tugitakayamensis*, *Cleyera japonica* and *Acer palmatum* var. *pubescens* (listed by decreasing dominance); and constant species include *Trochodendron aralioides*, *Neolitsea acuminatissima*, *Chamaecyparis obtusa* var. *formosana* and *Cleyera japonica* (listed by decreasing constancy). East-facing slope type (20 subplots) mainly distributes on the east-facing windward slopes. Diagnostic species include *Pourthiaea villosa* var. *parvifolia*, *Eurya glaberrima*, *Viburnum luzonicum*, *Quercus stenophylloides*, *Microtropis fokienensis*, *Osmanthus heterophyllus*, *Tetradium ruticarpum*, *Ilex sugerokii* var. *brevipedunculata*, *Itea parviflora*, *Litsea elongata* var. *mushaensis* and *Skimmia japonica* subsp. *distincte-venulosa*; dominant species include *Rhododendron formosanum*, *Quercus sessilifolia*, *Quercus longinix* and *Neolitsea acuminatissima*; and the constant species include *Symplocos macrostroma*, *Eurya crenatifolia*, *Rhododendron formosanum*, *Neolitsea acuminatissima*, *Quercus sessilifolia*, *Chamaecyparis obtusa* var. *formosana* and *Camellia brevistyla*. Finally, valley type (6 subplots) primarily distribute on the valley slope in the west part of LFDP. Diagnostic species include *Hydrangea angustipetala*; dominant species include *Quercus sessilifolia*, *Eurya crenatifolia*, *Cleyera japonica*, *Chamaecyparis obtusa* var. *formosana*, *Camellia*

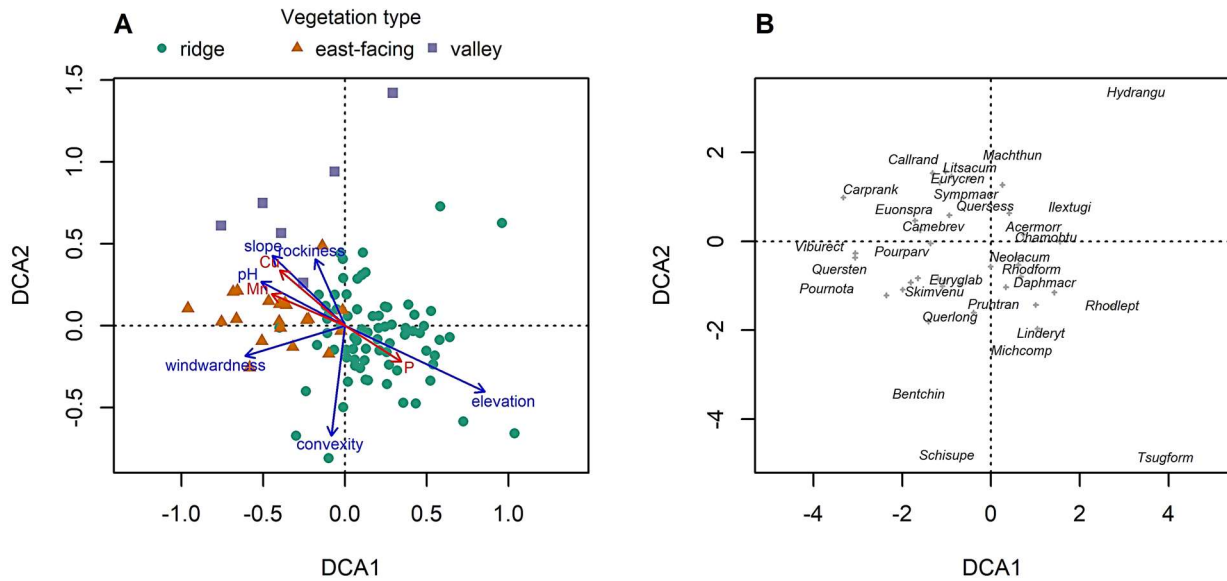


Fig. 5. DCA ordination diagrams, showing **A.** the relationships of the three vegetation types and environmental factors, passively projected onto the DCA ordination (blue vectors for variables measured in 100 subplots and significant at $P < 0.05$, red vectors for variables measured in 25 subplots and significant at $P < 0.1$), and **B.** scores of the more dominant species (for the meaning of abbreviations, see Supplement, Table S3).

brevistyla and *Acer palmatum* var. *pubescens*; and constant species include *Symplocos macrostroma*, *Eurya crenatifolia*, and *Quercus sessilifolia*.

When it comes to total species numbers, the ridge type contains 56 species and 3160 individuals, the east-facing slope type includes 51 species and 1941 individuals, and the valley type contains 25 species and 119 individuals. When considering structural characteristics of individual 10 m × 10 m subplots, the differences between the vegetation types are as follows. BA for the ridge type is, on average, 74.1 m² ha⁻¹ (11.3–191.6 m² ha⁻¹), for the east-facing slope type 63.1 m² ha⁻¹ (26.8–94.8 m² ha⁻¹), and for the valley type 27.4 m² ha⁻¹ (5.5–77.2 m² ha⁻¹), which is significantly lower than the other two types (Fig. S1A). The mean DBH for the ridge type is, on average, 15.8 cm (6.7–29.5 cm), for the east-facing slope type 9.8 cm (6.3–14.9 cm), and for the valley type 12.7 cm (6.1–26.5 cm), meaning that the ridge type is significantly higher than east-facing type, but valley type is not significantly different from the other two types (Fig. S1B). The density of individuals for ridge type is, on average, 42.7 individuals/100 m² (11–143), for east-facing slope type 97.1 individuals/100 m² (28–184), and for valley type 19.8 individuals/100 m² (14–30), with east-facing slope type being significantly higher than the other two types (Fig. S1C). Species richness of ridge type is, on average, 14 species (7–25), for east-facing type is 21.9 species (14–31), and for valley type is 11.3 species (7–16), with east-facing slope type being significantly species richer than the other two types (Fig. S1D). When considering BA of different leaf habit types (conifer, evergreen broadleaf and deciduous broadleaf), there are some consistent difference between vegetation types. Namely,

BA of coniferous species is significantly highest in the ridge type (27.6 m² ha⁻¹), while BA of evergreen broadleaf species is significantly highest in the east-facing slope type (56.9 m² ha⁻¹)(Fig. S1E–G). Considering differences in environmental variables between vegetation types (Fig. S2A–F), ridge type occurs in subplots with higher elevation and convexity, weaker windwardness, and lower soil rockiness and soil pH. East-facing slope type occurs in subplots with relatively lower elevation, high convexity, significantly higher windwardness, low soil rockiness and intermediate soil pH. Valley type occurs in subplots with lower elevation, negative convexity, low windwardness, higher soil rockiness, and higher soil pH. There are no significant differences in slope and soil depth between different vegetation types (Fig. S2C&G).

The result of DCA (Fig. 5, Table S2) shows the main gradients in species composition within the plot, the relationships between vegetation types, and also the relationship of vegetation patterns to environmental factors (passively projected onto the ordination diagram, Fig. 5A). The main gradient in species composition (the first DCA axis) is negatively related to windwardness and positively to elevation, and separates north-east facing vegetation types on windward slopes from the ridge vegetation type in relatively higher elevation within the plot. This pattern can be clearly observed when the site scores of individual subplots are visualised as a bubble diagram in the area of the plot (Fig. 6A). The second main gradient in species composition (the second DCA axis) is negatively related to convexity and positively to soil rockiness, and separates subplots of the valley vegetation type with concave topography and high soil rockiness,

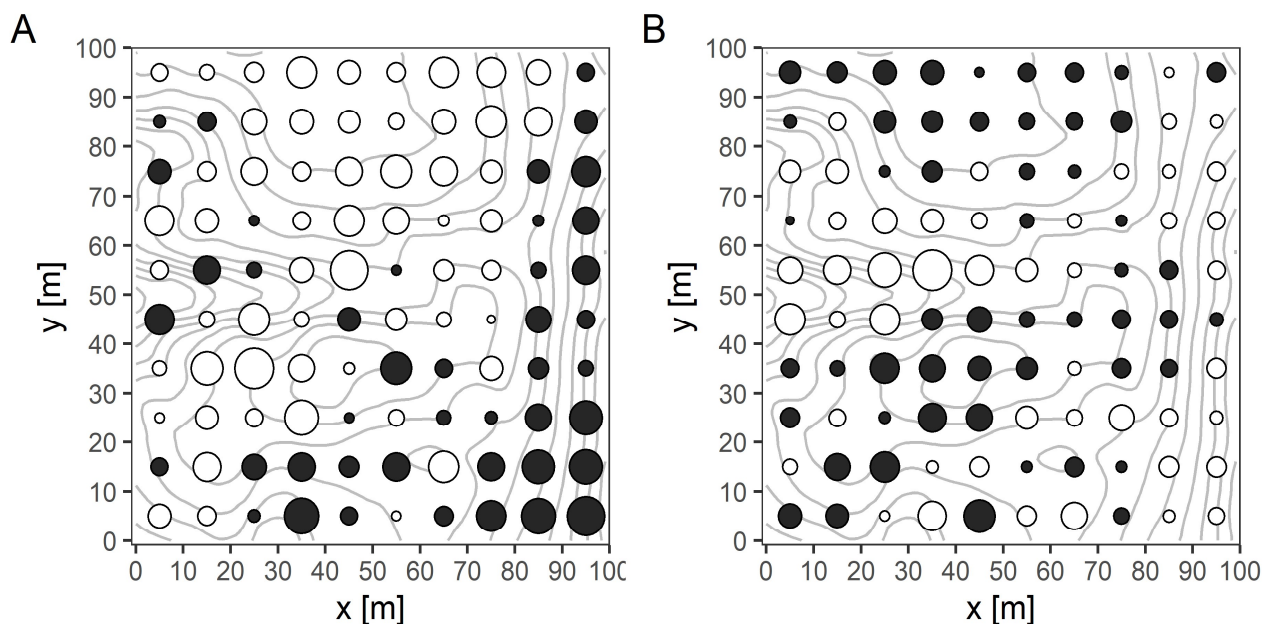


Fig. 6. Values of site scores along the first **A.** and second **B.** DCA axis, displayed in the space of the forest dynamics plot. The size of the bubble indicates absolute value of the score, the colour indicates negative (black) and positive (white) value.

from the flat or convex subplots of the other two vegetation types with lower or no soil rockiness (see also bubble diagram on Fig. 6B). The four soil variables significantly related to the first two DCA axes (pH, Cu, Mn and P) are separating valley type and partly also east-facing type with higher pH, Mn and Cu and lower P, from the ridge type with lower pH, Mn and Cu, but higher P.

For microclimate measured inside the LFDP between August 2021 and July 2023, the warmest month was July in 2022, with a mean temperature 19.2°C, and the coldest month was December in 2022, with a mean temperature 6.5°C (Fig. S4A). The daily temperature deviation between valley and flat ridge and between east-facing slope and flat ridge was generally lower than zero across a year except for November and February (Fig. S4B). Interestingly, during December and January, east-facing slopes affected by NE monsoon were slightly colder than both the flat ridge and the valley, while in the other parts of the year, both the valley and east-facing slopes were colder than the flat ridge, with valley colder than east-facing slope. The proportions of wet days (i.e. days with mean RH > 99%) from November to February were higher than 80% except for the flat ridge in February (Fig. S5A), and dry days (i.e. days with mean RH < 75%) were not frequent (Fig. S5B). The soil moisture between April 20, 2022, and May 20, 2022, increased along the topographical gradient from the convex ridge to the concave valley (Fig. S6).

DISCUSSION

Our data analysis shows that the variation (Fig. S7) in the composition of woody species in LFDP is driven by

two main environmental gradients, windwardness and convexity. Change of vegetation along windwardness gradient happens on compositional, diversity and physiognomic levels. Wind speed and direction measurements from the weather station beside the plot show that the prevailing wind in the area is from NE (50–60°), mainly because this is the overall direction of the winter monsoon. Windward east-facing slope vegetation type has the highest number of diagnostic species preferring this wind-affected habitat, has subplots with the highest richness and also with highest stem and branch density, creating dense but short canopy forest, which is being avoided by coniferous species but somewhat preferred by deciduous ones. It is commonly observed that forests become shorter and denser under the influence of chronic wind (Lawton, 1982). Similar dense stands can also be found in other windward-type forests in Taiwan affected by northeast monsoon, including the forest dynamics plots at Mt. Lopei (Lin *et al.*, 2005) and Lanjenchi (Chao *et al.*, 2007, 2010; Ku *et al.*, 2021). For completeness, we also have to acknowledge that the east-facing slope would be colder and wetter in general since it receives a relatively lower amount of solar radiation compared to parts of the plots facing south or southwest aspects. Also, the east-facing habitat includes the steepest quadrats in the whole dynamic plot, and the steepness itself can affect forest composition and physiognomy (Moeslund *et al.*, 2013). On the other side, the ridge vegetation type, which grows in less wind-affected and more convex habitats, has tall canopy, with dominance of coniferous *Chamaecyparis obtusa* var. *formosana*, and hosts trees with the largest DBH in the plot. The valley type occurs in a relatively small area, is concentrated into



convex habitats of dry gullies, and is characterised by low basal area, individual density and species richness of trees.

Temperature measurements from loggers in each of the three vegetation types showed that both east-facing and valley types, when compared to the ridge type, are relatively colder, mainly from March to September, and for windward sides also from November to February. This pattern probably reflects an interaction between the microclimate and topography of the three habitat types. Windward east-facing habitats are colder partly because of the cooling effect of wind (mostly in winter and spring during the winter monsoon period), but also because they receive solar radiation mostly during the morning hours, less so in the afternoon when they are already shaded. The valley type in a more topographically shaded position is generally less irradiated during the day and may also be affected by cold airflow at night. The ecological difference between convex and concave habitats is also strongly linked to soil moisture, as shown by our soil moisture measurements (Fig. S6). The concave sites in the southern and central part of the plot are filled with permanently wet mud (we call them pools of mud on the LFDP map in Fig. 2), and during rainy periods, they often get flooded.

Although soil variables are relatively poorly linked to species composition with only a few of them significant in the DCA and ANOVA analyses, several interesting patterns still appeared. Soil pH is consistently lowest in ridge vegetation type, probably for two reasons. First is the dominance of conifers in this habitat and, consequently, the accumulation of hard-to-decompose coniferous litter, leading to lower pH and higher C/N ratio in these subplots (Finzi *et al.*, 1998; Satti *et al.*, 2003; Hobbie *et al.*, 2006). The ridge type is also mostly on elevated flat ridges prone to leaching, removing cations from the soil and reducing soil pH. Interestingly, in the ordination diagram (Fig. 5A), phosphorus is negatively related to soil pH, which goes against the typical pattern where P is less available in soils with lower pH due to high levels of aluminium and iron cations, which combine with P and restrict its solubility (SanClements, 2010). We speculate that the negative correlation of P and pH in our plot results from the slow litter decomposition and accumulation of P in undecomposed organic material in a form unavailable for plants, especially convex subplots of ridge habitat in higher elevation dominated by conifers. Unpublished data from our small-scale application of resin soil probes (Plant Root Simulator, Western Ag. Innovations Inc., Saskatoon, Saskatchewan, Canada) in the plot during the 2022 season supports this interpretation. It showed that the supply rate of P anions in the soil in the six buried sets of probes is mostly (with exception of one measurement) below the method's detection limit ($0.2 \mu\text{g}/10\text{cm}^2/\text{burial length}$), indicating a possible P limitation. Finally, steeper subplots of east-facing and valley vegetation types tend to have higher concentrations of Cu

and Mn for reasons which remain unclear to us.

The low importance of soil properties to changes in species composition may be linked to several limitations of these measurements. Soil properties were measured only in 25 out of 100 subplots, and the reduced sample size also reduces the analytical power. However, since soil variables tend to be highly spatially autocorrelated on the scale of our observation, an even higher number of measurements may not improve the situation since the analysis would need to be adjusted for spatial autocorrelation. Also, we do not expect that overall variation in soil conditions between subplots within a relatively small area of the 1-ha plot is high enough to have a marked effect on vegetation, even though the plot's topography is relatively heterogeneous. And finally, the method of analysing the soil nutrients itself does not reflect their real availability for plants, but merely their concentration in the soil profile extracted by relevant chemical agents in the lab (Wilcke *et al.*, 2002; Axmanová *et al.*, 2011). Alternative methods may alleviate this problem, such as resin probes mentioned above or more elaborated ways of collecting and analysing the soil samples.

CONCLUSION

Our study provides data about the fine-scale species composition and spatial distribution of woody species in the 1-ha Lalashan Forest Dynamics Plot, an example of an old-growth stand belonging to the submontane *Chamaecyparis* mixed cloud forest. Our topographical, soil and microclimatic data show that the species composition here is mainly driven by the effect of wind and by topographical convexity, both having an impact on species composition, species richness and forest structure of the vegetation as well as soil and microclimatic conditions. The compositional and environmental data will serve as a reference for future resurveys to improve our understanding of the long-term dynamics and changes in montane cloud forest vegetation.

AUTHORS CONTRIBUTIONS

DZ and Ching-Feng Li (Woody) proposed the idea. TC, YNL together with DZ and other members of the Vegetation Ecology Lab and volunteers, established and surveyed LFDP. TC, YNL, and KSW maintained compositional and environmental data. YNL, TC and lab members from the Vegetation Ecology Lab and Soil Survey and Remediation Lab (of Prof. Zeng-Yi Hsu) analysed the soil samples. TC conducted the analyses of woody species composition and environmental factors data for the results, prepared the interpretation of results and discussion, and wrote the first draft of the manuscript as her Master thesis. PYL analysed microclimatic data and drew figures related to climate. DZ reanalysed and extended the manuscript, redrawn the figures, and prepared the final version of the text. All co-authors commented on the final version of the manuscript.



ACKNOWLEDGMENTS

We want to thank all members of the Vegetation Ecology Lab and other volunteers who participated in the field survey. We also greatly appreciate help from workers in Lalashan Recreation Area for help and a positive attitude toward our research expeditions. Thanks also go to the Taiwanese Forestry Bureau for renting us the abandoned weather station in the Lalashan Saddle. The research was financially supported by the Taiwanese Ministry of Science and Technology (MOST 106-2621-B-002-003-MY3 and MOST 109-2621-B-002-002-MY3) and Taiwanese National Science and Technology Council (NSTC 112-2621-B-002-004).

LITERATURE CITED

- Axmanová, I., Zelený, D., Li, C.-F., Chytrý, M.** 2011 Environmental factors influencing herb layer productivity in Central European oak forests: insights from soil and biomass analyses and a phytometer experiment. *Plant Soil* **342**(1-2): 183–194.
- Baker, D.E., Amacher, M.C.** 1982 Nickel, copper, zinc, and cadmium. In: Page, A.L. *et al.*, (Eds), *Methods of Soil Analysis, Part 2: Chemical and Microbiological Properties*, 2nd ed., Madison, WI: Soil Science Society of America, Inc. and American Society of Agronomy, Inc., pp. 323–336.
- Bergkvist, B., Folkesson, L., Berggren, D.** 1989 Fluxes of Cu, Zn, Pb, Cd, Cr, and Ni in temperate forest ecosystems. *Water Air Soil Pollut.* **47**(3-4): 217–286.
- Bruijnzeel, L.A., Scatena, F.N., Hamilton, L.S.** (eds) 2011 *Tropical Montane Cloud Forests: Science for conservation and management*. Cambridge: Cambridge University Press.
- Burt, R.** (Ed) 2004 *Soil Survey Laboratory Manual, Soil Survey Investigations Report, No. 42, Version 4.0*. Washington, DC: Natural Resource Conservation Service, US Department of Agriculture.
- Chao, W.-C., Chao, K.-J., Song, G.-Z. M., Hsieh, C.-F.** 2007 Species composition and structure of the lowland subtropical rainforest at Lanjenchi, southern Taiwan. *Taiwania* **52**(3): 253–269.
- Chao, W.-C., Song, G.-Z.M., Chao, K.-J., Liao, C.-C., Fan, S.-W., Wu, S.-H., Hsieh, T.-H., Hsieh, C.-F.** 2010 Lowland rainforests in southern Taiwan and Lanyu, at the northern border of Paleotropics and under the influence of monsoon wind. *Plant Ecol.* **210**(1): 1–17.
- Chou, C.-H., Chen, T.-Y., Liao, C.-C., Peng, C.-I.** 2000 Long-term Ecological Research in the Yuanyang Lake Forest Ecosystem I. Vegetation Composition and Analysis. *Bot. Bull. Acad. Sin.* **41**(1): 61–72.
- Chytrý, M., Tichý, L., Holt, J., Botta-Dukát, Z.** 2002 Determination of diagnostic species with statistical fidelity measures. *J. Veg. Sci.* **13**(1): 79–90.
- Condit, R.** 1998 *Tropical Forest Census Plots: Methods and results from Barro Colorado Island, Panama and a comparison with other plots*. Texas: Springer.
- Curtis, J.T.** (Ed) 1959 *The Vegetation of Wisconsin: An ordination of plant communities*. Madison, WI: University of Wisconsin Press.
- De Cáceres, M., Legendre, P., Valencia, R., Cao, M., Chang, L.-W., Chuyong, G., Condit, R., Hao, Z., Hsieh, C.-F., Hubbell, S., Kenfack, D., Ma, K., Mi, X., Noor, Md. N.S., Kassim, A.R., Ren, H., Su, S.-H., Sun, I.-F., Thomas, D., Ye, W., He, F.** 2012 The variation of tree beta diversity across a global network of forest plots. *Glob. Ecol. Biogeogr.* **21**(12): 854–864.
- Fajardo, A., McIntire, E.J.** 2010 Merged trees in second-growth, fire-origin forests in Patagonia, Chile: positive spatial association patterns and their ecological implications. *Am. J. Bot.* **97**(9): 1424–1430.
- Finzi, A.C., Breemen, N.V., Canham, C.D.** 1998 Canopy tree-soil interactions within temperate forests: species effects on soil carbon and nitrogen. *Ecol. Appl.* **8**(2): 440–446.
- Foster, P.** 2001 The potential negative impacts of global climate change on tropical montane cloud forests. *Earth-Sci. Rev.* **55**(1-2): 73–106.
- Gee, G.W., Bauder, J.W.** 1986 Particle-size analysis. In: Klute, A. (Ed), *Methods of Soil Analysis, Part 1: Physical and Mineralogical Methods*, 2nd edition. Madison, WI: Soil Science Society of America, Inc. and American Society of Agronomy, Inc., pp. 383–411.
- Granse, A., Führs, H.** 2013 Magnesium mobility in soils as a challenge for soil and plant analysis, magnesium fertilisation and root uptake under adverse growth conditions. *Plant Soil* **368**(1-2): 5–21.
- Hamilton, L.S., Juvik, J.O., Scatena, F.N.** (Eds) 1995 *Tropical Montane Cloud Forests*. New York: Springer-Verlag.
- Hill, M.O.** 1979 TWINSPLAN: A fortran program for arranging multivariate data in an ordered two-way table by classification of the individuals and attributes. Ithaca, New York: Ecology and Systematics, Cornell University.
- Hill, M.O., Gauch, H.G.** 1980 Detrended correspondence analysis: an improved ordination technique. *Vegetatio* **42**(1-3): 47–58.
- Hobbie, S.E., Reich, P.B., Oleksyn, J., Ogdahl, M., Zytkowski, R., Hale, C., Karolewski, P.** 2006 Tree species effects on decomposition and forest floor dynamics in a common garden. *Ecology* **87**(9): 2288–2297.
- Hsieh, C.-F., Chen, Z.-S., Sun, I.-F., Hsieh, T.-H., Zheng, Y.-B., Wang, K.-H., Su, M.-H., Jiang, F.-Y.** 1992 The subtropical rain forest in Nanjenshan Area, Kenting National Park (Report No. RES085) (Chinese). Taiwan: Kenting National Park, Construction and Planning Agency, Ministry of the Interior.
- Hu, J., Riveros-Iregui, D.A.** 2016 Life in the clouds: are tropical montane cloud forests responding to changes in climate? *Oecologia* **180**(4): 1061–1073.
- Hu, Y.-W., Tzeng, H.-Y.** 2019 Microhabitat types and tree species composition in an evergreen broadleaf forest at Mt. Peitungyen (Chinese). *Taiwan J. For. Sci.* **34**: 13–27.
- Huang, T.-C., Hsieh, C.-F.** 1994–2003 *Flora of Taiwan*, vol. I–IV, 2nd ed., National Taiwan University, Taipei.
- Ku, C.-C., Song, G.-Z. M., Chao, K.-J., Chao, W.-C.** 2021 Species-habitat associations of tree species under the northeast monsoon wind-affect tropical forest at Lanjenchi Forest Dynamics Plot, Taiwan. *Taiwania* **66**(1): 39–47.
- Ku, C.-C., Chao, K.-J., Song, G.-Z.M., Lin, H.-Y., Fan, S.-W., Chao, W.-C.** 2022 How the strength of monsoon winds shape forest dynamics. *Diversity* **14**(3): 169.
- Lai, I.-L., Chang, S.-C., Lin, P.-H., Chou, C.-H., Wu, J.-T.** 2006 Climatic characteristics of the subtropical mountainous cloud forest at Yuanyang Lake long-term ecological research site, Taiwan. *Taiwania* **51**(4): 317–329.
- Lawton, R.O.** 1982 Wind stress and elfin stature in a montane rain forest tree: an adaptive explanation. *Am. J. Bot.* **69**(8): 1224–1230.



- Lee, Y.-N. 2021 Importance of interspecific and intraspecific variation of plant functional traits: a case study in the Lashan Forest Dynamics Plot (dissertation). Taipei, Taiwan: Institute of Ecology and Evolutionary Biology, National Taiwan University. <https://doi.org/10.6342/NTU202104070>
- Legendre, P., Legendre, L. 2012 Numerical Ecology, Chapter 1.1: Spatial structure, spatial dependence, spatial correlation, 3rd ed., Oxford: Elsevier, pp. 8–21.
- Lepore, M., Arellano, G., Condit, R., Davis, S., Detto, M., Gonzalez-Akre, E. *et al.*, 2019 Fgeo: analyse forest diversity and dynamics. Available at: <https://cran.r-project.org/web/packages/fgeo/index.html> [Accessed July 30 2021]
- Li, C.-F., Chytrý, M., Zelený, D., Chen, M.-Y., Chen, T.-Y., Chiou, C.-R., Hsia, Y.-J., Liu, H.-Y., Yang, S.-Z., Yeh, C.-L., Wang, J.-C., Yu, C.-F., Lai, Y.-J., Chao, W.-C., Hsieh, C.-F. 2013 Classification of Taiwan forest vegetation. *Appl. Veg. Sci.* **16**(4): 698–719.
- Li, C.-F., Zelený, D., Chytrý, M., Chen, M.-Y., Chen, T.-Y., Chiou, C.-R., Hsia, Y.-J., Liu, H.-Y., Yang, S.-Z., Yeh, C.-L., Wang, J.-C., Yu, C.-F., Lai, Y.-J., Guo, K., Hsieh, C.-F. 2015 Chamaecyparis montane cloud forest in Taiwan: ecology and vegetation classification. *Ecol. Res.* **30**(5): 771–791.
- Lin, H.-Y., Yang, K.-C., Hsieh, T.-H., Hsieh, C.-F. 2005 Species composition and structure of a montane rainforest of Mt. Lopei in northern Taiwan. *Taiwania* **50**(3): 234–249.
- McIntire, E.J., Fajardo, A. 2011 Facilitation within species: A possible origin of group-selected superorganisms. *Am. Nat.* **178**(1): 88–97.
- Mulvaney, R.L. 1996 Nitrogen - inorganic forms. In: Sparks, D.L. *et al.*, Eds, *Methods of Soil Analysis, Part 3: Chemical Methods*. Madison, WI: Soil Science Society of America, Inc. and American Society of Agronomy, Inc., pp. 1123–1184.
- Nelson, D.W., Sommers, L.E. 1972 A simple digestion procedure for estimation of total nitrogen in soils and sediments. *J. Environ. Qual.* **1**(4): 423–425.
- Nelson, D.W., Sommers, L.E. 1996 Total carbon, organic carbon and organic matter. In: Sparks, D.L. *et al.*, Eds, *Methods of Soil Analysis, Part 3: Chemical Methods*. Madison, WI: Soil Science Society of America, Inc. and American Society of Agronomy, Inc., pp. 961–1010.
- Oksanen, J., Blanchet, F.G., Friendly, M., Kindt, R., Legendre, P., McGlinn, D. *et al.*, 2022 Vegan: community ecology package. Version 2.6-2. Available at <https://github.com/vegandevs/vegan> [Accessed December 17 2023]
- Ponco-Reyes, R., Reynoso-Rosales, V.H., Watson, J., VanDerWal, J., Fuller, R., Pressey, R., Possingham, H. 2012 Vulnerability of cloud forest reserves in Mexico to climate change. *Nat. Clim. Change* **2**(6): 448–452.
- Quervain, A.D. 1904 Die Hebung der atmosphärischen Isothermen in der Schweizer Alpen und ihre Beziehung zu deren Höhengrenzen. *Gerlands Beiträge zur Geophysik*, **6**, 481–533.
- R Core Team 2023 R: A Language and Environment for Statistical Computing. R Foundation for Statistical Computing, Vienna, Austria. <https://www.R-project.org/>
- Reinhardt, K., Smith, W.K. 2008 Impacts of cloud immersion on microclimate, photosynthesis and water relations of *Abies fraseri* Pursh. Poiret in a temperate mountain cloud forest. *Oecologia* **158**(2): 229–238.
- Rigueiro-Rodríguez, A., Mosquera-Losada, M.R., Ferreiro-Domínguez, N. 2012 Pasture and soil zinc evolution in forest and agriculture soils of Northwest Spain three years after fertilisation with sewage sludge. *Agric. Ecosyst. Environ.* **150**: 111–120.
- Roleček, J., Tichý, L., Zelený, D., Chytrý, M. 2009 Modified TWINSPAN classification in which the hierarchy respects cluster heterogeneity. *J. Veg. Sci.* **20**(4): 596–602.
- SanClements, M.D., Fernandez, I.J., Norton, S.A. 2010 Phosphorus in soils of temperate forests: linkages to acidity and aluminum. *Soil Sci. Soc. Am. J.* **74**(6): 2175–2186.
- Satti, P., Mazzarino, M.J., Gobbi, M., Funes, F., Roselli, L., Fernandez, H. 2003 Soil N dynamics in relation to leaf litter quality and soil fertility in north-western Patagonia forests. *J. Ecol.* **91**(2): 173–181.
- Schachtschabel, P. 1954 Das pflanzenverfügbare Magnesium des Bodens und seine Bestimmung. *Zeitschrift für Pflanzenernährung, Düngung, Bodenkunde* **67**(1): 9–23.
- Schulz, H.M., Li, C.-F., Thies, B., Chang, S.-C., Bendix, J. 2017 Mapping the montane cloud forest of Taiwan using 12 year MODIS-derived ground fog frequency data. *PLOS ONE* **12**(2): 1–17.
- Simpson, G.L. 2022 Permute: Functions for Generating Restricted Permutations of Data. R package version 0.9-7. Available at <https://CRAN.R-project.org/package=permute> [Accessed December 17, 2023]
- Song, G.-Z. 1996 The composition and distribution type in a warm temperate broad-leaved evergreen forest at Mt Peitungyen, central Taiwan dissertation Chinese. Taipei, Taiwan: Institute of Plant Biology, National Taiwan University.
- Song, G.-Z. M., Yang, K.-C., Hou, C.-H., Lin, J.-K., Hsieh, C.-F., Fan, S.-W., Chao, W.-C. 2010 Tree population dynamics over 12 yr in a warm temperate broad-leaved evergreen forest at Mt Peitungyen, central Taiwan. *Taiwan J. For. Sci.* **25**: 17–27.
- Stadtmüller, T. 1987 Cloud forest in the humid tropics. Costa Rica: The United Nations University.
- Still, C., Foster, P.N., Schneider, S.H. 1999 Simulating the effects of climate change on tropical montane cloud forests. *Nature* **398**(6728): 608–610.
- Su, H.-J. 1984 Studies on the climate and vegetation types of the natural forests in Taiwan II—Altitudinal vegetation zones in relation to temperature gradient. *Quarterly Journal of Chinese Forestry* **17**: 57–73.
- Tanner, E.V.J., Kapos, V., Freskos S., Theobald, A.M. 1990 Nitrogen and phosphorus fertilisation of Jamaican montane forest trees. *J. Trop. Ecol.* **6**(2): 231–238.
- Tichý, L. 2002 JUICE, software for vegetation science. *J. Veg. Sci.* **13**(3): 451–453.
- Tsui, C.-C., Chen, Z.-S., Hsieh, C.-F. 2004 Relationships between soil properties and slope position in a lowland rain forest of southern Taiwan. *Geoderma* **123**(1-2): 131–142.
- Turner, B.L., Romero, T.E. 2009 Short-term changes in extractable inorganic nutrients during storage of tropical rain forest soils. *Soil Sci. Soc. Amer. J.* **73**(6): 1972–1979.
- Urban, O., Janouš, D., Acosta, M., Marek, M.E. 2007 Ecophysiological controls over the net ecosystem exchange of mountain spruce stand. Comparison of the response in



- direct vs. diffuse solar radiation. *Glob. Change Biol.* **13**(1): 157–168.
- Valencia, R., Foster, R.B., Villa, G., Condit, R., Svenning, J.-C., Hernández, C., Romoleroux, K., Losos, E., Magard, E., Balslev, H.** 2004 Tree species distributions and local habitat variation in the Amazon: large forest plot in eastern Ecuador. *J. Ecol.* **92**(2): 214–229.
- von Uexküll, H.R., Mutert, E.** 1995 Global extent, development and economic impact of acid soils. *Plant Soil* **171**(1): 1–15.
- Walter, H., Lieth, H.** 1960 *Klimadiagramm Weltatlas*. G. Fischer, Jena, Germany.
- Wiesmeier, M., Urbanski, L., Hobbey, E., Lang, B., von Lützow, M., Marin-Spiotta, E., Wesemael, B., van Rabot, E., Ließ, M., Garcia-Franco, N., Wollschläger, U., Vogel, H.-J., Kögel-Knabner, I.** 2019 Soil organic carbon storage as a key function of soils - A review of drivers and indicators at various scales. *Geoderma* **333**: 149–162.
- Wilcke, W., Yasin, S., Abramowski, U., Valarezo, C., Zech, W.** 2002 Nutrient storage and turnover in organic layers under tropical montane rain forest in Ecuador. *Eur. J. Soil Sci.* **53**(1): 15–27.
- Zelený, D.** 2021 *twinspanR: TTwo-way INdicator SPecies ANalysis* and its modified version in R. Version 0.22. Available at <https://github.com/zdealveindy/twinspanR> [Accessed October 3 2021]

Supplementary materials are available from Journal Website